17. Phocaea family asteroids with measured reflectance spectra are: 25, 323, 326.
18. Asteroids greater than 60 km in diameter within 0.1 AU of the 2:1 Kirkwood gap with measured reflectance spectra include 92, 106, 108, 122, 175, 511, and 895.
19. NEA's 1580, 1685, 1943, 2201, and 1979VA have no meteoritic analogs; 1627 Ivar does not either, but its spectrum is too noisy to be useful; 433 is a stony-iron analog as judged by infrared spectra not addressed in this work; 1036 and 1620 have no meteoritic analogs, but spectral coverage is not sufficient to conclude that they are different in composition than any meteoritic type.
20. J. S. Lewis, *Space Sci. Rev.* **14**, 401 (1973).
21. J. Gradie and E. Tedesco, *Science* **216**, 1405 (1982); B. Zellner, in *Asteroids*, T. Gehrels, Ed. (Univ. of Arizona Press, Tucson, 1979), pp. 783–806; M. J. Gaffey and T. B. McCord, *Space Sci. Rev.* **21**, 555 (1978).
22. G. W. Wetherill, *Annu. Rev. Earth Planet. Sci.* **2**, 303 (1974).
23. C. R. Chapman, T. B. McCord, C. Pieters, *Astron. J.* **78**, 502 (1973); C. Pieters, M. J. Gaffey, C. R. Chapman, T. B. McCord, *Icarus* **28**, 105 (1976); M. A. Feierberg, H. P. Larson, C. R. Chapman, *Astrophys. J.* **257**, 361 (1982).
24. D. J. Tholen, thesis, University of Arizona, Tucson (1984).
25. M. J. Gaffey, *Icarus* **60**, 83 (1984).
26. V. F. Buchwald in *Handbook of Iron Meteorites* (Univ. of California Press, Berkeley, 1975), pp. 15–25; Z. Ceplecha and R. E. McCrosky, *J. Geophys. Res.* **81**, 6257 (1976).
27. P. R. Weissman and G. W. Wetherill, *Astron. J.* **79**, 404 (1974); R. S. Dunbar, thesis, Princeton University, Princeton (1980).
28. Supported by the Space Foundation of Houston, Texas, and NASA grants NSG 7323, NSG 7312, and NAGW 562. We thank G. W. Wetherill, L. A. Lebofsky, and an anonymous reviewer for their comments.

10 October 1984; accepted 8 March 1985

Phytoplankton Blooming Off the U.S. East Coast: A Satellite Description

Abstract. *A "bloom" of near-surface phytoplankton occurs in the Atlantic Slope region of the western Atlantic Ocean off the U.S. East Coast in the spring. Satellite time series of sea-surface temperature and phytoplankton pigment concentration, derived from measurements of the National Oceanic and Atmospheric Administration NOAA-7 Advanced Very-High-Resolution Radiometer and the National Aeronautics and Space Administration Nimbus-7 Coastal Zone Color Scanner, respectively, give information on the spatial extent and temporal development of such a bloom for a 28-day period in April through May 1982. The phytoplankton concentration of the slope area is comparable to that of the Atlantic Shelf. Total primary productivity of the slope during this period is equivalent to that of the shelf. The primary productivity within a warm-core ring and in the Gulf Stream system is less by a factor of 2.*

O. B. Brown
R. H. Evans
J. W. Brown
Division of Meteorology and Physical Oceanography, Rosenstiel School of Marine and Atmospheric Science, University of Miami, Miami, Florida 33149
H. R. Gordon
Department of Physics, University of Miami, Coral Gables, Florida 33124
R. C. Smith
Marine Bio-Optics Group, University of California at Santa Barbara, Santa Barbara 93106
K. S. Baker
Marine Bio-Optics Group, University of California at San Diego, La Jolla 92093

The "spring bloom" is a biological phenomenon that occurs during the temperate-zone transition from winter to spring in which phytoplankton are observed to grow rapidly. It is a dramatic example of the direct response of an oceanic biological process to changes in the physical environment. The classical explanation for the spring bloom was given by Riley (*1, 2*) and Sverdrup (*3*). During the winter, the breakdown of vertical stratification and the associated deep vertical mixing cause increased amounts of nutrients to be transferred into the euphotic zone. However, the same process cycles phytoplankton out of and into this zone (which is shallow in winter because of the reduced solar radiation incident on the sea surface). As a result, in winter the phytoplankton experience average light levels that are too low to allow net productivity in the water column, in spite of the elevated nutrient concentrations in the euphotic zone. The onset of the seasonal stratification, due to the warming of the surface waters in the spring, limits the vertical mixing to the upper tens of meters; this restricts the vertical movement of phytoplankton, for the most part, to the euphotic zone. Phytoplankton are then able to utilize this light- and nutrient-rich environment to reproduce in large numbers, thus blooming or flowering in a short period of time.

Typically, the concentration of chlorophyll *a* is used as an indicator of phytoplankton biomass because of the ease with which this quantity can be measured fluorometrically (*4*). In work with color imagery, however, the sum of the near-surface concentrations of chlorophyll *a* and pheopigments (henceforth referred to as the pigment concentration) is used as an index of phytoplankton biomass. At the pigment concentrations encountered, it should make no appreciable difference whether one uses the chlorophyll *a* concentration or the pigment concentration since the pheopigment concentration is typically only 10 percent or less of the chlorophyll *a* concentration (*5, 6*), which is well below the inherent error in our satellite-derived estimate of the pigment concentration (*7*).

Satellite imagery provides a synoptic view of the ocean surface over large areal extents and extended time periods, an accomplishment that was not possible with traditional oceanographic measurements. In the past, efforts have been made to acquire a time series of a particular region from repeated ship visits to single sites. For example, Menzel and Ryther (*8*) reported the results of one of the few complete long-term biological time series in the northwestern Sargasso Sea. They found that the chlorophyll *a* concentration in near-surface waters reached peak levels (1 mg m^{-3}) in early spring, dropped during the summer to 0.1 mg m^{-3}, rose slightly in the fall (0.5 mg m^{-3}), and then dropped again in late fall. However, they were not able to observe evolution of the spatial structure from their single station. Ryther and Yentsch (*9*) presented a biomass time series for the Atlantic Slope and the Atlantic Shelf, which indicated a bloom in the slope region (to 2 mg m^{-3}) during April. Their data (*9*) showed a major bloom (7 mg m^{-3}) on the shelf in February and March. Cox *et al.* (*10*) computed vertical profiles of chlorophyll on a monthly basis for the northern Sargasso Sea and the slope region. They found surface values in the slope waters of 0.45 mg m^{-3} in March, with maximum values of 2.9 mg m^{-3} in late April; these results underscore the difference in the timing and the magnitude of blooms in different regions off the U.S. East Coast. O'Reilly and Busch (*11*) presented data that emphasize the wide variety of blooms in subregions of the northwestern Atlantic Shelf waters. The slope region they examined was a narrow band near the shelf break, which reached a productivity maximum (1.5 g of carbon per square meter per day) in April and May whereas during the rest of the year it was half this amount.

The new satellite technology can provide a comprehensive overview of the surface temperature and pigments in several regions of the open ocean simultaneously. Data for four areas are presented here, including selected areas of the shelf, the slope, the Gulf Stream, and a

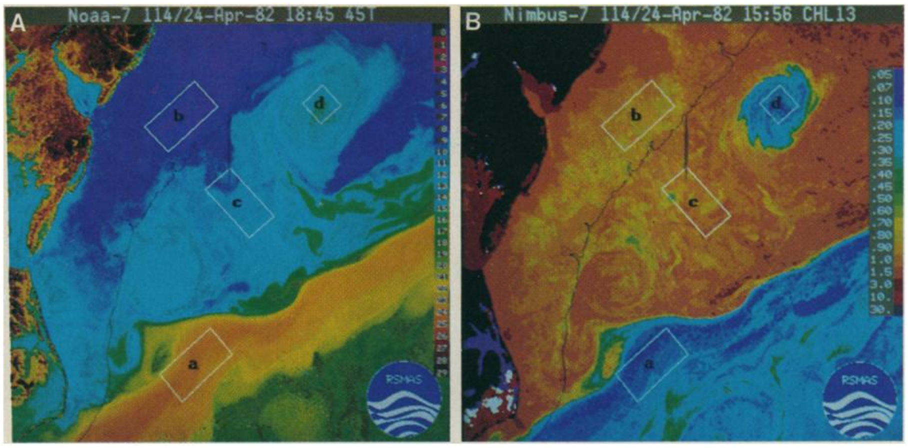

Fig. 1. (A) Processed Advanced Very-High-Resolution Radiometer image of the U.S. East Coast on 24 April 1982 (temperature ranges from 5° to 25°C); (B) processed Coastal Zone Color Scanner image of the U.S. East Coast on 24 April 1982 (phytoplankton pigment concentration, ranging from 0.05 to 10.0 mg m^{-3}, is scaled logarithmically from low to high concentrations). Representative sample boxes are shown on the shelf (region b), in the slope (region c), in a warm-core ring (region d), and in the Gulf Stream (region a). A second warm-core ring is located north of region a, and a cold-core ring is located southeast of region a. The 200-m isobath is included in both photographs.

warm-core ring. Warm-core rings (WCR) are anticyclonic features with a mean diameter of about 100 km that exist within the slope area for an average of 6 months; these WCR's move 3 to 5 km day^{-1} in a southwesterly direction. During three WCR experiment cruises (*12*) in April–May, June, and August 1982, we investigated WCR 82-B and the surrounding regions. Ship measurements of surface temperature and pigment concentration from the spring WCR experiment were used to validate the satellite-derived counterparts (*13*).

The thermal measurements used for determining sea-surface temperature (SST) were derived from the National Oceanic and Atmospheric Administration (NOAA) satellite series Advanced Very-High-Resolution Radiometer (AVHRR) instrument (*14*). Ideally, one determines the SST by measuring the apparent radiance of the ocean in the AVHRR infrared channels and converting this radiance to temperature, using Planck's blackbody formula. However, the apparent radiance is subject to several environmental factors, which degrade the accuracy of the perceived temperature. Major sources of error are sun glint from the surface, which increases the radiance in AVHRR channel 3, and water vapor absorption in the lower atmosphere, which decreases the radiance in AVHRR channels 4 and 5. In the present work a multispectral technique was used for the water vapor correction (*15*). The effects of varying water vapor concentrations on the integrated atmospheric transmittance over each of the three infrared channels differ; consequently, algorithms for the correction of water vapor–induced absorption in each channel can be constructed, which depend on the differences in the perceived SST between pairs of channels (*16, 17*).

The visible (pigment) measurements were derived from the Coastal Zone Color Scanner (CZCS) on the National Aeronautics and Space Administration (NASA) experimental satellite Nimbus-7 (*18*). One determines pigment concentration by measuring the radiance diffusely reflected from the ocean in the blue and green spectral regions. Waters low in phytoplankton pigments reflect more blue light than green, whereas waters high in pigments reflect more green light as a result of the selective absorption of blue light by the pigments (*19*). As in the case of the infrared measurements, the apparent radiance at the satellite differs from that at the sea surface. Typically as much as 50 to 90 percent of the radiance measured at the satellite in the visible arises from the backscattering of solar radiation from the atmosphere. This radiance must be removed before the pigment concentration can be estimated. We used the method of Gordon and Clark (*6*) with the clear-water modifications of Gordon and Clark (*20*) and a sensitivity degradation (*21*) to correct the visible imagery.

We mapped an area extending from 70°W to 76°W, 35°N to 40°N, into a 1-km matrix, using atmospherically corrected satellite retrievals. The original infrared data set included two images per day from NOAA-7, with overpass times at approximately 0300 and 1500 local time (*22*). An area twice the size of the desired target area was processed to obtain SST and was then remapped to the standard grid to compensate for satellite orbit and scanner characteristics (*23*). The resulting temperature map is spatially located to ±1 km over the entire image. Temperatures are processed in 0.125°C steps and contoured in 1°C increments. An example of such an SST map for the area under investigation is shown in Fig. 1A. A comparison between the satellite-derived SST and the water temperature measured continuously along the ship track for Julian day 120 is shown in Fig. 2A. Because the ship location changes as a function of time, the satellite pixel (picture element) corresponding to the ship's latitude and longitude has been extracted.

Fourteen useful CZCS images were available in the spring bloom interval from April through May 1982. The CZCS data were navigated and geometrically processed by the procedures used for AVHRR. Figure 1B is a processed CZCS image for the same day as the thermal image in Fig. 1A. The shelf and slope are higher in pigment than the Gulf Stream, which is visible in the lower right part of the image.

The validity of general chlorophyll algorithms (*19*) for the onset of this particular bloom was established through use of shipboard measurements (*24, 25*) made in April and May 1982 as part of the WCR program (*12*). Figure 2B shows one example of the comparison of pigment concentrations derived from shipboard-calibrated fluorescence taken at 1-minute intervals along track for Julian day 120 with those calculated from the CZCS data (*26*). In general, the entire pigment image series comparison shows a level of agreement similar to that seen in Fig. 2B, that is, to within a factor of 2 (satellite low) for this spring bloom period.

The relation of the along-track ship surface pigment measurement, C_0, to that integral of pigment over a depth of one attenuation length, C_K, as seen from the satellite (*27–29*) is affirmed in Fig. 3 through use of shipboard vertical profile data. Moreover, the degree to which this satellite-measured chlorophyll is representative of the water column is demonstrated in Fig. 4, where C_K is plotted against the pigment integrated over the whole euphotic zone, C_T. These ship data regressions are statistical means over the April cruise interval. There is good agreement with earlier data (*5*) obtained from a variety of stations in the Southern California Bight. In spite of this agreement, it must be recognized that this relation probably varies both seasonally and regionally.

The satellite images in Fig. 1 under-

Table 1. Satellite-derived pigments (C_K and C_T) and productivity (P_T) values with error estimates. Error estimates are based on the assumption that present algorithm inaccuracy is a factor of 2. Daily estimates are halved, doubled, and integrated, respectively, to produce a range for each parameter. This range is used to derive the error estimates.

Region	$<\overline{C}_K>$ (mg m^{-3})	$<\overline{C}_T>$ (mg m^{-2})	Area (10^{11} m^2)	$C^i = \iint C_T dt dA$ (10^5 metric tons)	$C^i/\Sigma C^i$ (%)	$<\overline{P}_T>$ (mg m^{-2} day^{-1})	$\iint P_T dt dA$ (10^6 metric tons)
Shelf	2.8 ± 1.7	65.7 ± 15.5	1.2	2.21 ± 0.52	46	924 ± 118	3.11 ± 0.40
Slope	3.0 ± 1.8	65.5 ± 14.4	1.2	2.20 ± 0.48	45	917 ± 103	2.82 ± 0.32
Warm-core ring	0.5 ± 0.3	28.9 ± 11.5	0.1	0.08 ± 0.03	2	529 ± 159	0.30 ± 0.09
Gulf Stream	0.3 ± 0.2	21.2 ± 9.0	0.6	0.35 ± 0.15	7	423 ± 138	0.71 ± 0.23

score the difficulty associated with quantifying the meaning of an average temperature or pigment concentration for any one particular region, since no region is strictly isolated from any other. To obtain a quantitative measure of parameters in this initial study, a rectangular box (40 by 80 km) was defined for each region except the WCR itself, which was sampled with a box 33 by 33 km. The sizes and orientations of these regions are adjusted to mask the effects of clouds. The Gulf Stream box region, region a in Fig. 1, remained centered near 36°N, 73°W, with the major axis aligned with the Gulf Stream core. For the slope region, region c in Fig. 1, the center position of the box moved about the center area, 38°N, 73°W, to avoid such events as Gulf Stream meanders, but the major axis remained perpendicular to the shelf break. For the shelf region, region b in Fig. 1, the box center was established at 39°N, 74°W, with the major axis aligned parallel to the shelf break (200-m isobath). The WCR was sampled with the box, region d in Fig. 1, remaining centered on the ring and oriented to reside within the ring's high-velocity region.

The resulting average temperature and pigment found within the sampling boxes for each of the defined areas from the Nimbus-7 CZCS and NOAA-7 AVHRR are plotted versus time in Fig. 5, A through D. The occurrence of the spring bloom is immediately apparent in the plots of pigment concentration, with definite variations in magnitude and timing in each of the regions.

Bloom magnitude. Flowering onset was apparent at the beginning of the time series (8 April 1982). Blooming in the ring occurred in two intervals of approximately 10 days each, with pigment concentrations less than 0.6 mg m^{-3}; pigment concentrations increased a second time in ring waters during the latter part of the bloom time interval for the shelf and slope. Gulf Stream waters exhibited a single short-lived event during April. In shelf and slope waters, much larger pigment concentrations (>2 mg m^{-3}) were found, with a 4-week duration for the bloom. The bloom extended at its peak throughout the area from 35°N to 40°N. One can make an areal estimate of the total chlorophyll, using the information shown in Fig. 3, by converting C_K to C_T per square meter (*5*). The time integral of this result over the bloom period gives the total chlorophyll for each region per square meter. Multiplying each regional chlorophyll value by its areal extent and then summing all the regions gives the total chlorophyll for this East Coast region over the bloom period. Table 1 gives regional sums and the standard error. Because of the nonlinear relation between the variables listed in Table 1, the parameters are derived on a daily basis and are then integrated over time to produce the mean values given.

The bloom is considered to have lasted from Julian day 104 to Julian day 132; this is the range used for the integration of all quantities listed in Table 1. Also given is the ratio of each regional chloro-

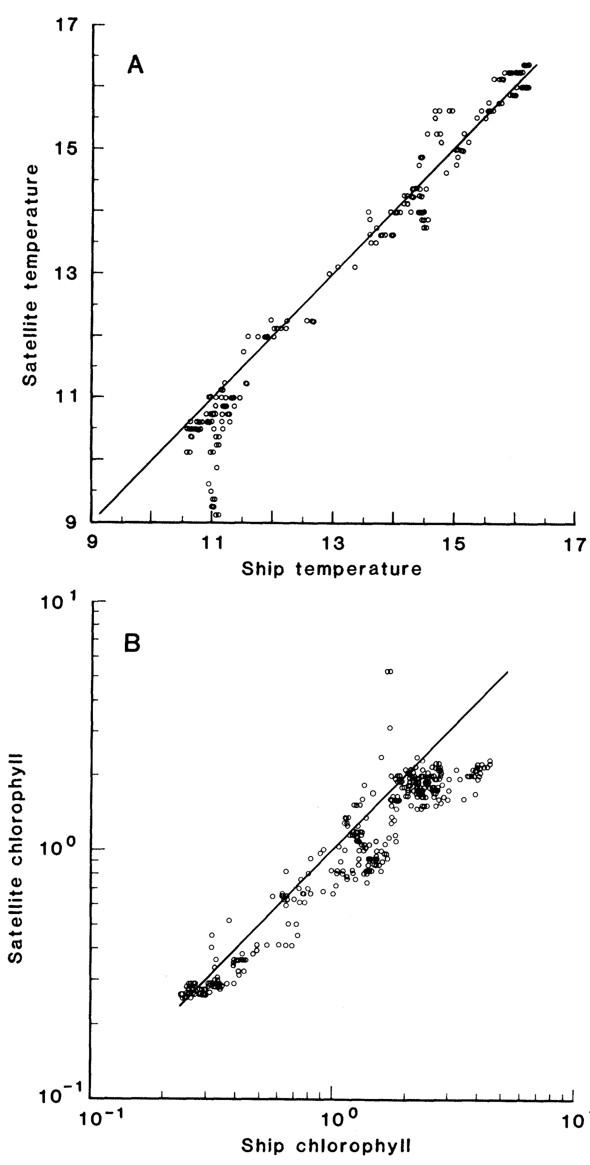

Fig. 2. Comparison between the satellite-determined and ship-measured sea-surface temperature (A) and pigment concentration (B) for Julian day 120 in the vicinity of warm-core ring 82-B.

phyll value to the total chlorophyll during this bloom period. For the sum of shelf, slope, rings, and Gulf Stream, 46 percent of the total optically weighted pigment was found on the shelf and 45 percent was located on the slope (Table 1). This equivalence between slope and shelf contributions to pigment concentrations might not have been predicted from historical data.

Gulf Stream and ring pigment concentrations were lower, but the euphotic depth is much greater, therefore, C_T values were reduced by much less than might be expected from C_K ratios. Optically weighted total pigment concentrations were lower by factors of 3 and 5 in the ring and in the Gulf Stream, respectively, than on the shelf or slope.

Historical data from the Sargasso Sea (*8, 10*) and observations from the shelf (*9, 10, 30*) are consistent with these results for the Gulf Stream and shelf systems, respectively. The shelf result is within the range found by Walsh (*30*) for open shelf and riverine-dominated shelf in the Mid-Atlantic Bight.

Bloom timing. The concurrent use of temperature and chlorophyll imagery allows one to consider the mechanism responsible for the bloom in each area. The temperature time series indicates that the seasonal warming and the bloom itself have different cycles. Seasonal warming was seen in the shelf region during the flowering event, whereas there was little change in the surface temperature field in the slope waters, the ring, and the Gulf Stream during this period.

Conventional wisdom suggests that a spring bloom occurs when the winter nutrient-rich, deep-mixed water column becomes stratified such that phytoplankton do not mix out of the euphotic depth and a bloom is sustained (*3*). We can infer such stratification from the satellite imagery for the shelf since the color imagery shows a bloom in the pigment and the infrared imagery records increasing temperature at the beginning of seasonal warming, indicative of reduced mixing (Fig. 5). Shipboard in situ data confirm this observation. For the slope region, however, although the color imagery shows a bloom, the temperature change is not evident. We can conclude either that the bloom mechanism differs or that the stratification mechanism is similar but the temperature increase is too small to be observed from space. One expects the surface thermal warming to be less in the slope region than in the shelf region since the mixed-layer depth is considerably greater on the slope than on the shelf. This same argument is also relevant for the Gulf Stream and ring environments. One would expect the buildup of vertical stratification to be slower in these areas. Alternatively, it could be assumed that, although thermal warming is not yet observed, strong vertical mixing may have ceased, which would permit bloom onset. The bloom in the ring had two maxima; a storm event occurred from Julian day 117 to Julian day 118, which apparently destroyed the stratification, but, once stratification was reestablished, bloom development was again evident.

Primary productivity. One must use chlorophyll concentrations as a general

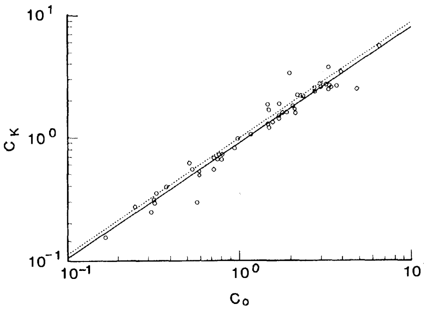

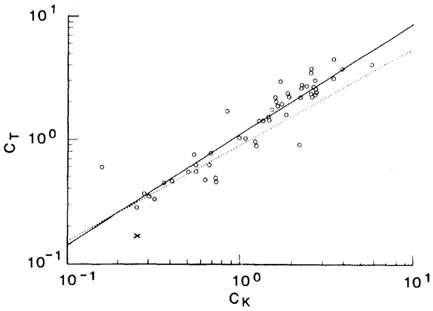

Fig. 3 (left). Shipboard vertical profile data integrated to show the relation between the logarithm of the average pigment concentration (in milligrams per cubic meter) to a depth of 1 attenuation depth (K), C_K, versus the logarithm of the average pigment concentration of the surface, C_0; C_0 represents the pigment value routinely determined by shipboard along-track measurements, whereas C_K represents the pigment concentration as determined from satellite imagery. A linear regression through this data gives $\log C_K = -(0.03 \pm 0.011) + (0.946 \pm 0.0278) \log C_0$ (solid line), which compares with the relation found by Smith and Baker [figure 3 of (*5*)] of $\log C_K = -(0.031 \pm 0.010) + (0.961 \pm 0.016) \log C_0$ (dashed line). Fig. 4 (right). Relation derived from shipboard vertical profile data of pigment concentration (in milligrams per cubic meter) integrated to a depth of 1 attenuation length (K), C_K, versus pigment concentrations integrated over the entire euphotic zone, C_T. A linear regression through this data gives $\log C_T = (0.040 \pm 0.017) + (0.892 \pm 0.047) \log C_K$ (solid line), which can be compared with the relation found by Smith and Baker [figure 4 in (*5*)] of $\log C_T = -(0.02 \pm 0.017) + (0.788 \pm 0.021) \log C_K$ (dashed line).

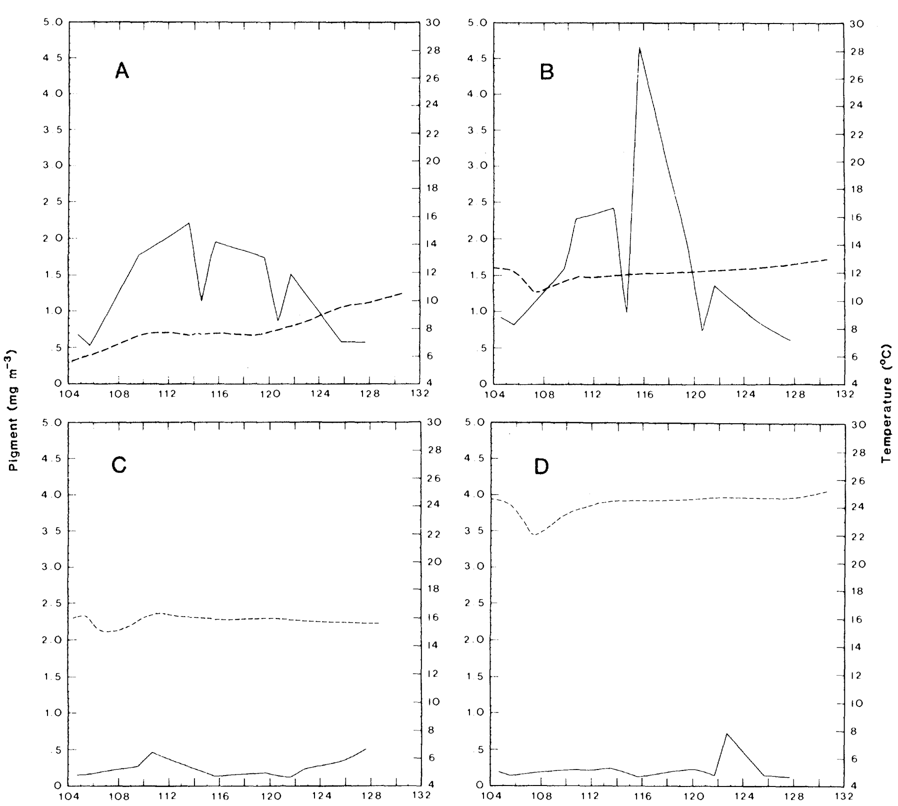

Fig. 5. Temperature (dashed line) and pigment (solid line) time series for four selected regions along the U.S. East Coast, including the shelf (A), the slope (B), a warm-core ring (C), and the Gulf Stream (D). The locations of these regions are shown in Fig. 1.

index of primary productivity with caution, although on a regional scale the two components are recognized as coherent (*31–34*). In an investigation of the productivity index in the Southern California Bight, Smith and Baker (*35*) found

$$\log P_T = 1.254 + 0.728 \log C_K$$

where P_T is the productivity (in milligrams of carbon per square meter per day) as measured on the ship. This equation presents a possible methodology for deducing regional productivity. We must emphasize that the satellite only detects upwelling spectral radiation from a depth of approximately 1 optical attenuation length, K. Inferences beyond this $1/K$ depth (in meters) to the 1 percent light level ($4.6/K$) depth are based upon regressions (*5, 36*) derived from ship vertical-profile data. Use of the above regression, although inexact, does permit a comparison of productivity in these regions. The last two columns of Table 1 give P_T integrated over the bloom period per square meter per day and the areally integrated result, respectively. The area shoreward of the 200-m isobath between Cape Hatteras and 70°W constitutes the shelf region, and the area between the mean location of the northern edge of the Gulf Stream (*37*) and the 200-m isobath constitutes the slope region for the calculation in Table 1. The calculated productivity integrated per meter square is comparable for the slope and the shelf, whereas the values for the ring and Gulf Stream are less by a factor of 2. These data are in agreement with the available ^{14}C determinations of primary productivity (*38*). The total productivity in clear waters can be within a factor of 2 of that observed in the much more eutrophic waters because of the vertical weighting by euphotic depth, which is part of this calculation. If the P_T-C_K relationship were exact, then, based on the estimated upper limit to the error in C_K, the P_T estimates should be within 15 percent for the shelf and slope and within 30 percent for the clearer waters.

References and Notes

1. G. A. Riley, *J. Mar. Res.* **5**, 67 (1942).
2. ———, *ibid.* **6**, 54 (1946).
3. H. U. Sverdrup, *J. Cons. Cons. Perm. Int. Explor. Mer* **18**, 287 (1953).
4. T. Platt, K. L. Denman, A. D. Jassby, in *The Sea*, E. D. Goldberg *et al.*, Eds. (Wiley, New York, 1977), pp. 807–856.
5. R. C. Smith and K. S. Baker, *Limnol. Oceanogr.* **23**, 247 (1978).
6. H. R. Gordon and D. K. Clark, *Boundary-Layer Meteorol.* **18**, 299 (1980).
7. H. R. Gordon *et al.*, *Appl. Opt.* **22**, 20 (1983).
8. D. W. Menzel and J. H. Ryther, *Deep-Sea Res.* **6**, 351 (1960).
9. J. H. Ryther and C. S. Yentsch, *ibid.* **3**, 327 (1958).
10. J. L. Cox *et al.*, *Biol. Oceanogr.* **1**, 271 (1982).
11. J. E. O'Reilly and D. A. Busch, *Rapp. P.-V. Reun. Cons. Int. Explor. Mer* **183**, 255 (1984).
12. Warm Core Rings Executive Committee 1982, *EOS* **63**, 834 (1982).
13. T. Joyce, "ENDEAVOR 83 Cruise Report" (Woods Hole Oceanographic Institute, Woods Hole, Mass., April 1982).
14. A. Schwalb, *The TIROS-N/NOAA A-G Satellite Series* (Publ. NOAA TM NESS 95, Government Printing Office, Washington, D.C., 1978).
15. E. P. McClain *et al.*, *Adv. Space Res.* **2**, 43 (1982); A. E. Strong and E. P. McClain, *Bull. Am. Meteorol. Soc.* **65**, 138 (1984).
16. D. Anding and R. Kauth, *Remote Sensing Environ.* **1**, 217 (1970).
17. C. Prabhakara, G. Dalu, V. G. Kunde, *J. Geophys. Res.* **79**, 1744 (1974).
18. W. A. Hovis *et al.*, *Science* **210**, 60 (1980).
19. H. R. Gordon and A. Morel, *Remote Assessment of Ocean Color for Interpretation of Satellite Visible Imagery: A Review* (Springer, New York, 1983).
20. H. R. Gordon and D. K. Clark, *Appl. Opt.* **20**, 4175 (1981).
21. H. R. Gordon *et al.*, *ibid.* **22**, 3929 (1983).
22. O. B. Brown *et al.*, *Univ. Miami Rosenstiel School Mar. Atmos. Sci. Tech. Rep. No. 81004* (1981).
23. O. B. Brown and R. H. Evans, *Nav. Res. Rev.* **34**, 7 (1982).
24. ———, in preparation; R. C. Smith and K. S. Baker, *J. Geophys. Res.*, in press.
25. R. C. Smith *et al.*, *Appl. Opt.* **23**, 2791 (1984).
26. R. C. Smith *et al.*, *Fluorometric Techniques for the Measurement of Oceanic Chlorophyll in the Support of Remote Sensing* (Ref. 81-17, Scripps Institution of Oceanography, La Jolla, Calif., 1981).
27. H. R. Gordon and W. R. McCluney, *Appl. Opt.* **14**, 413 (1975).
28. ———, D. K. Clark, *ibid.* **19**, 3428 (1980).
29. R. C. Smith, *Mar. Ecol.* **5**, 359 (1981).
30. J. J. Walsh, *Prog. Oceanog.* **12**, 1 (1983).
31. O. J. Koblentz-Mishke, V. V. Valkovinsky, J. C. Kabanova, in *Scientific Exploration of the South Pacific*, W. S. Wooster, Ed. (National Academy of Sciences, Washington, D.C., 1970), pp. 183–193.
32. J. J. Walsh, Ed., "MAREX, The Marine Resources Experiment, Report of the Ocean Color Science Working Group" (Publ. 1983-397-034, Government Printing Office, Washington, D.C., 1983).
33. T. Platt and A. W. Herman, *Int. J. Remote Sensing* **4**, 343 (1983).
34. R. W. Eppley, E. Stewart, M. R. Abbott, U. Heyman, *J. Plankton Res.* **7**, 57 (1985).
35. R. C. Smith and K. S. Baker, *Mar. Biol.* **66**, 267 (1982).
36. R. C. Smith *et al.*, *ibid.*, p. 281.
37. C. D. Parker, *Deep-Sea Res.* **18**, 981 (1971).
38. G. L. Hitchcock, C. Langdon, T. J. Smayda, *ibid.*, in press.
39. R. C. Smith and K. S. Baker, *The Bioptical State of Natural Waters and Remote Sensing* (Ref. 77-2, Scripps Institution of Oceanography, La Jolla, Calif., 1977).

40. We acknowledge the work of S. Emmerson and A. Li in the computer software and navigation generation. We thank D. Olson, J. McCarthy, and W. Esaias for insightful comments and encouragement. This research is part of the Warm Core Rings Experiment sponsored by the National Science Foundation–Division of Ocean Sciences. The Nimbus Project at Goddard Space Flight Center, Beltsville, Md., provided CZCS data in near real time. The National Oceanic and Atmospheric Administration–National Environmental Satellite and Data Information Service Operations and Research Groups made arrangements and provided manpower for the near real time acquisition of the NOAA-7 AVHRR infrared data. Supported under National Science Foundation grant OCE-80-16991; National Aeronautics and Space Administration grant NAGW-273, grant NAGW-290-2, and contract NAS 5-22963; and Office of Naval Research contract N000-80-C-0042.

19 November 1984; accepted 29 April 1985

A Large Deletion Within the T-Cell Receptor Beta-Chain Gene Complex in New Zealand White Mice

Abstract. *The T-cell receptor β-chain gene complex contains a duplication of D_β, J_β, and C_β gene segments in mice and man. When DNA from many inbred strains of mice was screened an unusual allele of the beta locus was identified in New Zealand White (NZW) mice. This allele is distinguished by the deletion of an 8.8-kilobase segment of DNA containing $C_{\beta 1}$, $D_{\beta 2}$ and the $J_{\beta 2}$ cluster. Despite the fact that all NZW T-cell receptors must be derived from a single set of β-chain gene segments, this strain has functional T cells and is phenotypically normal. This deletion of T-cell receptor β-chain segments occurs in a strain known to contribute to lupus-like autoimmune disease.*

Brian L. Kotzin
Department of Medicine, V.A. Medical Center, Denver, Colorado 80220, and Departments of Medicine and Microbiology and Immunology, University of Colorado Health Sciences Center, Denver 80262
Virginia L. Barr
Edward Palmer*
Department of Medicine, National Jewish Hospital and Research Center, Denver, Colorado 80206, and Department of Microbiology and Immunology, University of Colorado Health Sciences Center

*To whom correspondence should be addressed.

New Zealand White (NZW) mice have generated interest because of their role in the autoimmunity of New Zealand Black (NZB) × NZW F_1 hybrids. Although NZB mice develop an autoimmune hemolytic anemia as the major feature of their autoimmune disease, NZB × NZW F_1 mice exhibit (i) marked antibody production to nuclear antigens, (ii) high serum levels of antibodies to double-stranded DNA, and (iii) a fatal immune-complex glomerulonephritis (*1*). These features are similar to those observed in human systemic lupus erythematosus (SLE). Despite their genetic contribution to NZB × NZW F_1 autoimmunity, NZW mice are phenotypically normal and they have normal life spans (*2*). The basis of their genetic contribution to the F_1 disease has not been determined (*3*).

T-lymphocyte antigen receptors restricted to the major histocompatibility complex (MHC) are disulfide-linked het-